JOURNAL OF APPLIED PHYSICS **115**, 014504 (2014)

Electron-beam-induced current at absorber back surfaces of Cu(In,Ga)Se_2 thin-film solar cells

J. Kavalakkatt,[1] D. Abou-Ras,[1,a)] J. Haarstrich,[2] C. Ronning,[2] M. Nichterwitz,[1] R. Caballero,[1,b)] T. Rissom,[1] T. Unold,[1] R. Scheer,[1,c)] and H. W. Schock[1]
[1]*Helmholtz-Zentrum Berlin für Materialien und Energie, Hahn-Meitner-Platz. 1, 14109 Berlin, Germany*
[2]*Institut für Festkörperphysik, Friedrich Schiller Universität Jena, Max-Wien-Platz 1, 07743 Jena, Germany*

(Received 1 October 2013; accepted 10 December 2013; published online 7 January 2014)

The present work reports on investigations of the influence of the microstructure on electronic properties of Cu(In,Ga)Se_2 (CIGSe) thin-film solar cells. For this purpose, ZnO/CdS/CIGSe stacks of these solar cells were lifted off the Mo-coated glass substrates. The exposed CIGSe backsides of these stacks were investigated by means of electron-beam-induced current (EBIC) and cathodoluminescence (CL) measurements as well as by electron backscattered diffraction (EBSD). EBIC and CL profiles across grain boundaries (GBs), which were identified by EBSD, do not show any significant changes at Σ3 GBs. Across non-Σ3 GBs, on the other hand, the CL signals exhibit local minima with varying peak values, while by means of EBIC, decreased and also increased short-circuit current values are measured. Overall, EBIC and CL signals change across non-Σ3 GBs always differently. This complex situation was found in various CIGSe thin films with different [Ga]/([In]+[Ga]) and [Cu]/([In]+[Ga]) ratios. A part of the EBIC profiles exhibiting reduced signals across non-Σ3 GBs can be approximated by a simple model based on diffusion of generated charge carriers to the GBs. © *2014 AIP Publishing LLC*.
[http://dx.doi.org/10.1063/1.4858393]

I. INTRODUCTION

Thin-film solar cells with polycrystalline Cu(In,Ga)Se_2 (CIGSe) absorbers reach high power conversion efficiencies of up to 20.4%.[1,2] A thickness of the CIGSe absorber of approximately 2 μm is sufficient for the absorption of most of the incoming light because of the high absorption coefficient of CIGSe of about 10^5 cm^{-1} for visible light.[3] This helps to reduce the material consumption and correspondingly the production costs.

The influences of structural defects in the CIGSe absorber layer on the photovoltaic performances of corresponding solar cells have still not been fully understood. Due to the presence of higher concentrations of point defects, leading to subgap states, grain boundaries (GBs) are in general expected to feature higher recombination rates of generated charge carriers. However, the local short-circuit current at the position of a GB in a polycrystalline CIGSe thin film, as acquired by means of electron-beam-induced current (EBIC) measurements on cross-section specimens, does not seem to be reduced substantially.[4] In some cases, even higher EBIC signals at GBs than in grain interiors are reported.[5,6] Up to now, EBIC measurements at GBs in CIGSe solar cells have been performed mostly in the cross-section configuration, which allows for analysis of a rather limited specimen area with few GBs. However, EBIC data from cross-section specimens of CIGSe solar cells can be described well,[4,7] using a linear model first published by Donolato.[8] It should be noted that, recently, the charge-carrier collection in the CIGSe solar cells was reported to be dependent on the generation,[9] which has to be taken into account when applying this linear model.

EBIC measurements on backsides of ZnO/CdS/CIGSe absorbers, which provide information on the charge-carrier collection from much larger areas, have already been reported by Scheer *et al.*[10] However, this study localized GBs only by means of contrasts in scanning electron microscopy (SEM) images, which is not an unambiguous detection of GBs, since these images contain also contrasts related, e.g., to surface roughnesses and impurities.

In the present work, a ZnO/CdS/$CuInSe_2$ (CISe) and a ZnO/CdS/CIGSe stack were investigated by means of SEM techniques on the backsides of the CI(G)Se layers, which were exposed by delamination of the Mo/glass substrates from the complete solar-cell stacks. Thus, large measurement areas were accessible. By means of EBIC and cathodoluminescence (CL) measurements, charge-carrier collection and radiative recombination in the grain interiors and at GBs of the CI(G)Se absorber layers were investigated. In addition, electron backscatter diffraction (EBSD) maps were acquired on the identical positions as the EBIC and CL signals, which gave the means to localize and to classify GBs unambiguously.[11,12] The linear model developed by Donolato,[8] modified by the authors with respect to the different measurement configuration used in the present work, was applied to extract local values for diffusion lengths and recombination velocities at GBs.

II. EXPERIMENTAL DETAILS

The CIGSe solar cells for the present work were produced at the Helmholtz-Zentrum Berlin. In a three-stage

a)Author to whom correspondence should be addressed. Electronic mail: daniel.abou-ras@helmholtz-berlin.de
b)Present address: Universidad Autónoma de Madrid, Departamento de Física Aplicada, c/ Fransisco Tomás Valiente 7, 28049 Madrid, Spain.
c)Present address: Martin Luther-Universität Halle-Wittenberg, Institut für Physik, FG Photovoltaik, 06099 Halle, Germany.

TABLE I. Compositional ratios of the CIGSe thin films, as well as the photovoltaic parameters of the corresponding solar cells studied in the present work, where V_{oc} is the open-circuit voltage, j_{SC} the short-circuit current density, FF the fill factor, and η the power-conversion efficiency.

[Ga]/([In]+[Ga])	[Cu]/([In]+[Ga])	V_{oc} (mV)	j_{sc} (mA/cm^2)	FF (%)	η (%)
0	0.82	490	36.9	73	13.1
0.28	0.83	674	31.1	71	14.8

physical vapor-deposition process,[13] the CISe and CIGSe absorber layers (2 μm) were deposited on Mo-coated soda-lime glass substrates. The solar cells were completed by chemical-bath-deposited CdS (50 nm), by a sputtered ZnO/ZnO:Al bilayer as front contact (500 nm), and by an evaporated Ni/Al contact-grid. Compositional ratios and solar-cell parameters of the CI(G)Se layers in the investigated solar cells are given in Table I.

After deposition of a graphite layer (serving as diffusion barrier for Ag in the epoxy glue) on the ZnO/ZnO:Al front contact, the solar-cell stack was glued by use of Ag epoxy glue to an Al sample holder (Fig. 1). The backside of the CIGSe absorber layer was exposed by lifting off the Mo-coated glass substrate. In order to passivate the CIGSe (back) surface and to enhance the conductivity, a graphite layer was evaporated on top. EBIC measurements were performed by using a contact wire (Cu-Sn alloy) on the CIGSe surface as back contact. The front contact was realized via a contact wire connected to the Al sample holder, which is connected to the ZnO:Al layer of the solar cell via the Ag epoxy glue. The electron beam current I_B was measured by use of a faraday cup.

Spatial distributions of the current I_{EBIC} (EBIC images) were recorded in short-circuit condition at room temperature using a Femto DLPCA 200 transimpedance amplifier, while EBSD maps were acquired at 20 kV and 10 nA by use of an Oxford Instruments HKL NordlysII detector and of the CHANNEL5 software suite, both at a LEO GEMINI 1530 scanning electron microscope. CL images were obtained at 8 kV and 250 pA using a JEOL SEM 6490 microscope and a Gatan monoCL3 system with a monochromator and an (In,Ga)As photomultiplier Hamamatsu R5509-73, which was cooled to 193 K. The sample was placed on a liquid-He-cooled cryo-stage, leading to sample temperatures of about 8 K.

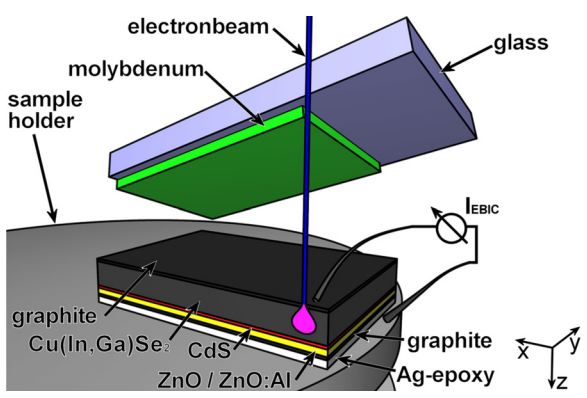

FIG. 1. Preparation and measuring geometry for EBIC measurements on CIGS back surfaces.

III. THEORETICAL DETAILS

The collection of charge carriers in a solar cell absorber can be described by a simple model. Donolato[14] assumed the current I_{EBIC} of a p-n junction for low-injection conditions to be a convolution of a generation function $g(\vec{x})$ and a collection function $f_c(\vec{x})$

$$I_{EBIC} = \int_V g(\vec{x}) f_c(\vec{x}) dV, \tag{1}$$

where V is the volume of the quasineutral region (QNR), which ranges from the boundary of the space-charge region (SCR) to the back contact with a certain surface recombination velocity. For the CIGSe absorber layer in the solar cell, the collection function $f_c(\vec{x})$ can be deduced from the continuity equation for minority charge carriers (electrons in a p-type semiconductor) by applying the reciprocity theorem as described by Donolato:[14] $D_n \Delta f_c(\vec{x}) + \mu_n \vec{E} \vec{\nabla} f_c(\vec{x}) - f_c(\vec{x})/\tau = 0$. D_n is the diffusion constant for electrons in the CIGS absorber, which is assumed to be about 2.5 cm^2/s (from Einstein's relationship $D_n = \mu_n k_B T/e$, with μ_n the electron mobility, about 100 cm^2/Vs,[15] $k_B T$ the thermal energy and e the elemental charge). Furthermore, τ is the lifetime of the electrons, and $\vec{E}$ denotes the electric field.

The collection function $f_c(\vec{x})$ is equivalent to the probability to collect a charge carrier, which is generated at position $\vec{x}$. This is, the generated electron diffuses to the edge of the SCR, and then drifts and diffuses to the front contact, where it is collected and contributes to the measured current. It is assumed that within the SCR, all generated electrons are collected ($f_c(\vec{x}_{SCR}) = 1$), and furthermore that the solar cell is translation-invariant parallel to the p-n junction, such that a reduction to one dimension is valid. The direction perpendicular to the p-n junction is described by z.

For an infinite semiconductor layer, where $f_c(z) \to 0$ for $z \to \infty$ and $f_c(z_{SCR}) = 1$ at the edge of the SCR, the solution is an exponential function $f_c(z) = \exp[-z/L]$, where length $L = \sqrt{D_n \tau}$ is the diffusion length of the minority-charge carriers. A semiconductor with finite thickness, as the absorber layer in a CIGSe solar cell, is limited by a back contact at position z_{BC}. The boundary condition of the collection function at the back contact is $\frac{d}{dx} f_c(z_{BC}) = (\frac{S_{BC}}{D_n}) f_c(z_{BC})$,[14] with the recombination velocity S_{BC} of minority charge carriers at the back contact. A solution for the collection function $f_c(z)$ is

$$f_c(z) = \frac{\frac{1}{L}\cosh\left(\frac{z - z_{BC}}{L}\right) - \frac{S_{BC}}{D_n}\sinh\left(\frac{z - z_{BC}}{L}\right)}{\frac{1}{L}\cosh\left(\frac{z_{BC} - z_{SCR}}{L}\right) - \frac{S_{BC}}{D_n}\sinh\left(\frac{z_{BC} - z_{SCR}}{L}\right)}. \tag{2}$$

Fig. 2 represents this collection function $f_c(z)$ for various recombination velocities s_{BC} and diffusion lengths L. The positions of the back contact and of the edge of the SCR, z_{BC} and z_{SCR}, are at 0 and at 2 μm.

The generation function g in Eq. (1) is determined from Monte-Carlo simulations.[16,17] It depends on the average

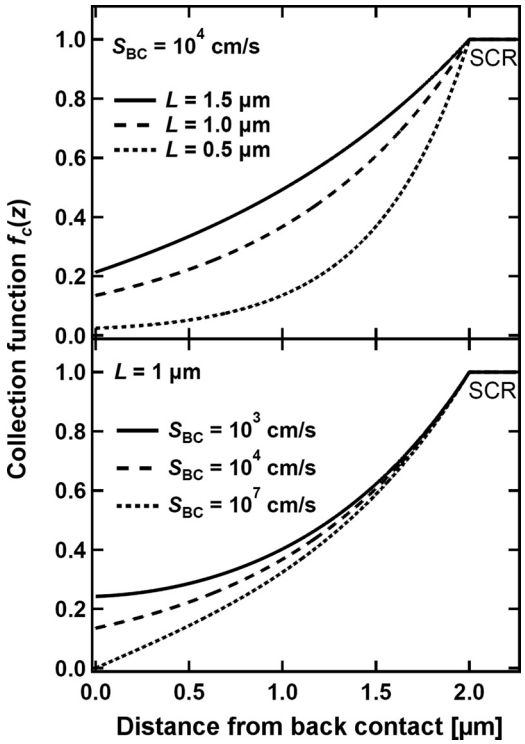

FIG. 2. Collection function $f_c(z)$ calculated by use of Eq. (2) for a CIGSe solar cell with (a) a constant recombination velocity at the back contact and varied diffusion length and (b) with a constant diffusion length and varied recombination velocity at the back contact.

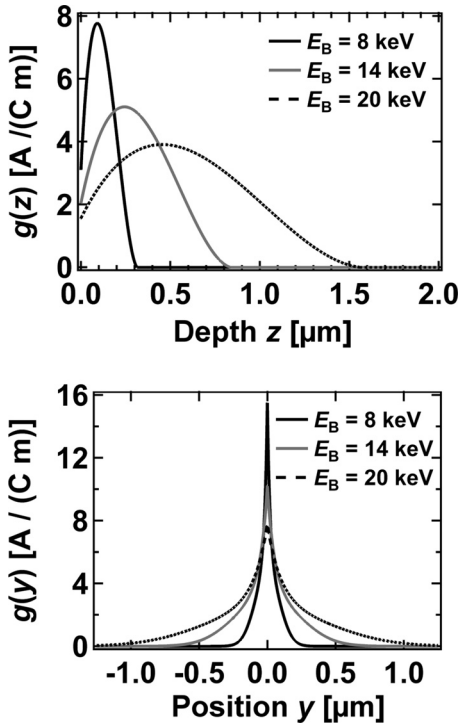

FIG. 3. One-dimensional generation functions $g(z)$ and $g(y)$ for CIGSe absorbers and various acceleration energies of the electron beam E_B.

density of the irradiated material and on the energy E_B of the electron beam. The one-dimensional generation functions for the depth ($g(z)$) and lateral ($g(y)$) directions are shown in Fig. 3 for a CIGSe thin film (assumed density of 5.75 g/cm^2). With higher energy E_B, the penetration depth into the material as well as the lateral extension of the generation profile increase.

In the present work, GBs are considered surfaces with recombination velocities S_{GB}, neglecting substantial accumulation of charges and also changes in composition, both affecting the energy-band diagram at the surface. An effective diffusion length L_{eff} can be determined depending on the distance y to the surface (i.e., the GB)[8]

$$L_{\mathrm{eff}}(y) = L\sqrt{1 - \frac{\frac{S_{\mathrm{GB}}}{D_n}L}{\frac{S_{\mathrm{GB}}}{D_n}L + 1}\int g(y)\exp\left(-\frac{y}{L}\right)dy}. \quad (3)$$

Due to the lateral generation function $g(y)$, the diffusion length L_{eff} depends on the acceleration energy E_B. For the simulation of the EBIC signal I_{EBIC} at a GB, L is substituted by L_{eff} in Eq. (2). In this case, the collection function $f_c(y,z)$ depends also on the distance y to the GB.

In Fig. 4, the simulated currents for various acceleration energies E_B and recombination velocities S_{GB} are shown. For increasing E_B, the EBIC value at the GB decreases less strongly, and the width of the profile increases. For increasing recombination velocities S_{GB}, the EBIC decreases more strongly.

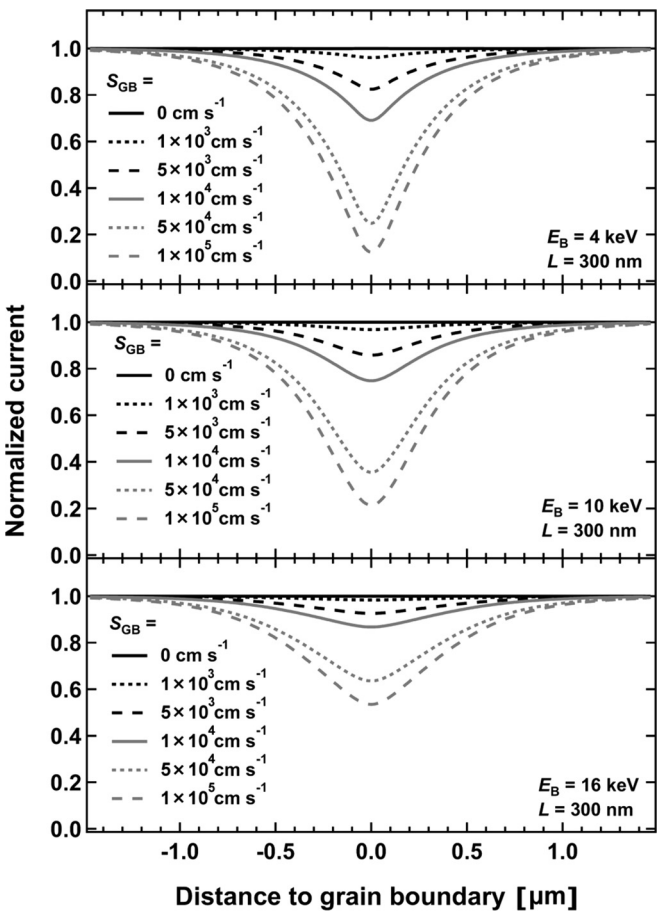

FIG. 4. Simulated and normalized currents at GBs for various acceleration energies E_B as well as recombination velocities S_{GB} at GBs. The diffusion length of minority charge carriers L was set to 300 nm.

IV. EXPERIMENTAL RESULTS AND DISCUSSIONS

A. Contrast changes in EBIC images

EBIC images from backsurfaces of CIGSe layers exhibit various positions at which the signal changes substantially (Fig. 5). These positions can be attributed directly to the presence of GBs (reduced EBIC signal), which can be identified and classified by means of EBSD (see Sec. IV E).

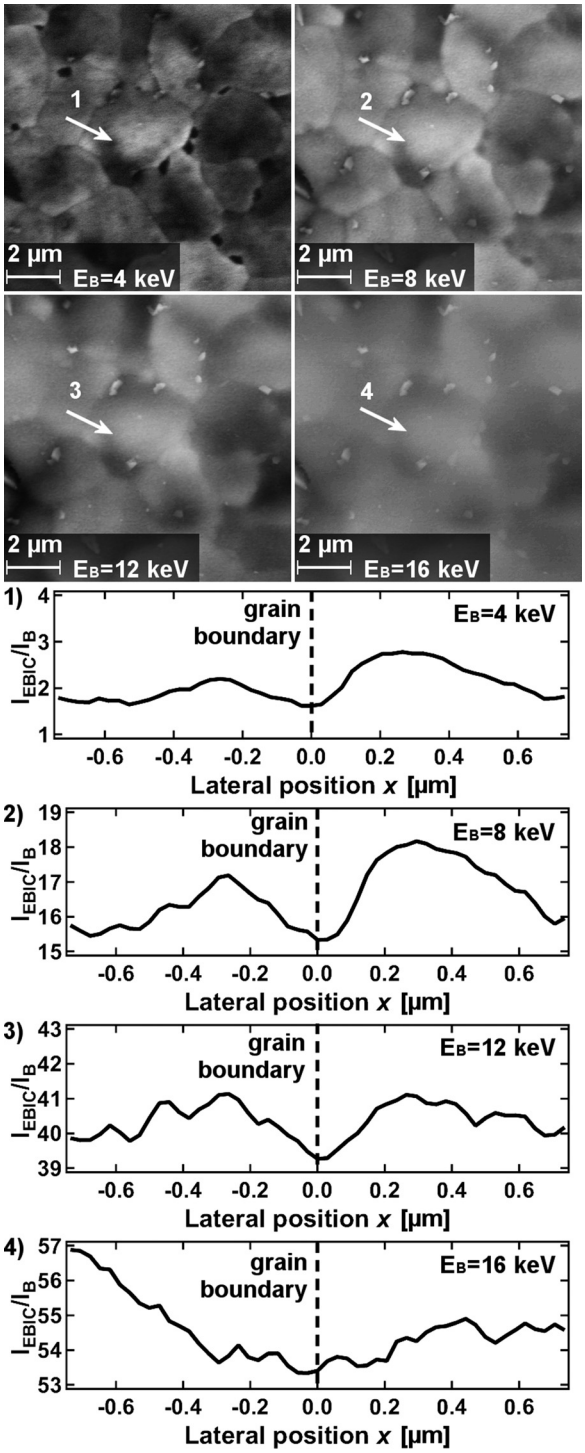

FIG. 5. EBIC images of a $CuInSe_2$ thin film acquired on its back surface using $E_B = 4$, 8, 12, and 16 keV, and profiles extracted at the positions highlighted by the arrows. The grey values of the EBIC images correspond to the measured short-circuit current.

Cavities and roughnesses resulting from the lift-off of the Mo/glass substrate are also visible in the EBIC images in Fig. 5, which lead to increases (cavities, pits) or decreases (bumps) of the EBIC value.

B. Influence of the electron-beam energy E_B

Measured EBIC images at one position at the back surface of a $CuInSe_2$ thin film with electron-beam energies of $E_B = 4$, 8, 12, and 16 keV are shown in Fig. 5. At low electron-beam energies ($E_B = 4$ keV), the contrasts in the EBIC image can be attributed to the microstructure of the CISe layer, see Sec. IV E below. Correspondingly, the dark lines between the individual grains can be attributed to positions of GBs.

In comparison to the EBIC images measured at $E_B = 8$ keV, the signal to noise ratio is lower for $E_B = 4$ keV. This finding can be attributed to smaller generation depths at lower E_B (Fig. 3(a)), since under such a condition, the charge carriers are generated closer to the surface, i.e., the probability that they recombine at the surface before they are collected is higher. For acceleration energies higher than 8 keV (Fig. 5), the EBIC signal at the GBs becomes smeared out owing to the increased generation volume (at 8 keV, the penetration range of the impinging electron beam is about 300 nm (Ref. 18)). With increasing energies, the influence of surface recombination is reduced, while the EBIC and the information depth increase. Furthermore, the EBIC signals from CIGSe back surfaces are projections of signals from a three-dimensional, polycrystalline material system, in which GBs are generally not oriented perpendicularly but at arbitrary angles with respect to the back surfaces. This fact is another possible source of diffuse signals at GBs.

C. Influence of irradiation by the electron beam

During the irradiation by the electron beam, the values of the EBIC signals and also the contrast at the GBs changed. Fig. 6(a) shows the EBIC image of a CISe/CdS/ZnO stack in the beginning and Fig. 6(b) after irradiation for 30 min at a low electron-beam energy of $E_B = 5$ keV and an electron-beam current of 125 pA. The profiles extracted from the normalized EBIC image, I_{EBIC}/I_B, across a GB before and after this irradiation (Fig. 6 bottom) show a changed EBIC value as well as a different shape of the profile. The average current decreased by more than 50%, and the local minimum in the current distribution across the GB changed its shape from asymmetric to symmetric. This effect is reversible. The EBIC values and the profiles across the GBs relax back to the starting condition after storing the sample for a few days in darkness.

For high electron-beam energies of $E_B \geq 16$ keV, an increase of the current is found after irradiation for 30 min. This effect is also reversible. Unfortunately, it is not possible to determine the behavior of the EBIC signal at the GB for these beam energies, because of the vanishing signal for high generation volumes (see above). The effects upon irradiation of the backside of the ZnO/CdS/CISe stack may be related to metastable states induced by charge-carrier trapping and a consequent change of the local effective doping density in

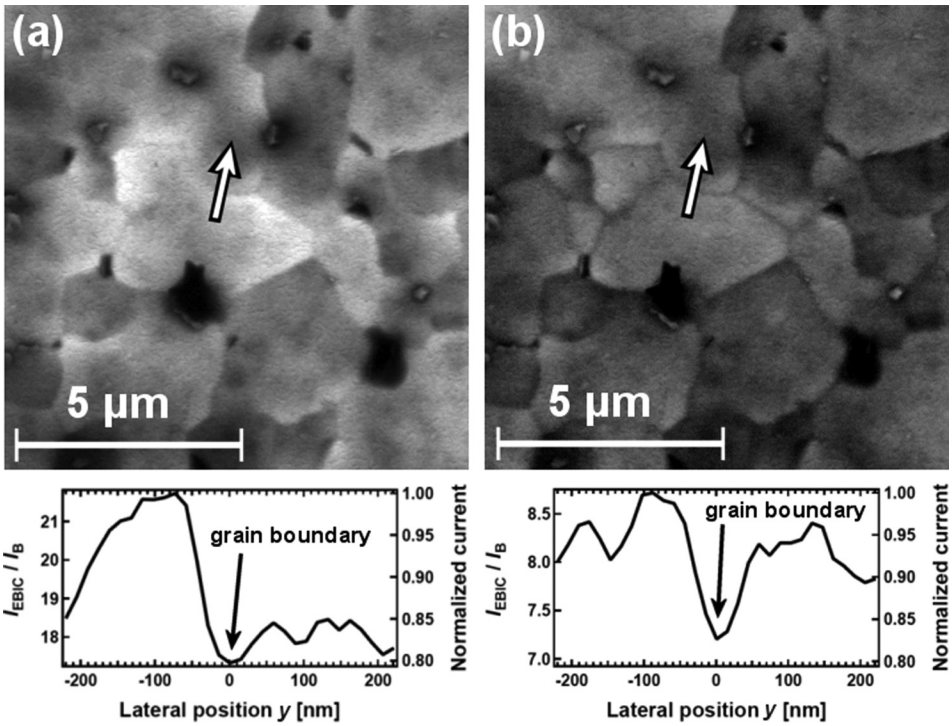

FIG. 6. EBIC images of a ZnO/CdS/CISe layer (a) in the beginning of the measurement and (b) after irradiation with the electron beam ($E_B = 5$ keV, $I_B = 125$ pA) for 30 min as well as extracted profile across the grain boundary.

the CISe layer.[19–21] In case these changes are only induced in the quasi-neutral region of the absorber layer, because of a small generation depth for low electron-beam energies, the effect on charge-carrier collection can be a different one than for higher electron beam energies with generation also in the space-charge region and at the heterojunctions of the solar cell. This may explain the differences in EBIC signal found after 30 min of irradiation at 5 and 16 keV.

D. Different EBIC profiles across various GBs

In Fig. 7, various profiles extracted from EBIC images across GBs in CIGSe (Fig. 7(a)) and CISe (Fig. 9(b)) thin films without irradiation by the electron beam are shown. There is no general behavior of the EBIC signal found for all the GBs investigated. At most GBs, the current exhibits a local minimum, with different minimum values. At some GBs, the EBIC is increased substantially with respect to the grain interiors. Asymmetric as well as symmetric EBIC distributions were found.

For GBs with enhanced EBIC signals with respect to the grain interiors (found at several GBs on both, CISe and CIGSe backsurfaces), the current increases from both sides towards the GB, where the increase of the EBIC value starts in a distance of about 1000 nm from the GB. In addition, a local minimum in the EBIC signal is visible at the position of the GB, which exhibits a full width at half maximum of 50 to 100 nm. These shapes of the EBIC signals around GBs may be attributed to two effects on charge carriers with two different length scales (about 1 μm and 50–100 nm). While EBIC profiles across GBs with local minima at the position of the GB can be simulated by use of the theory introduced

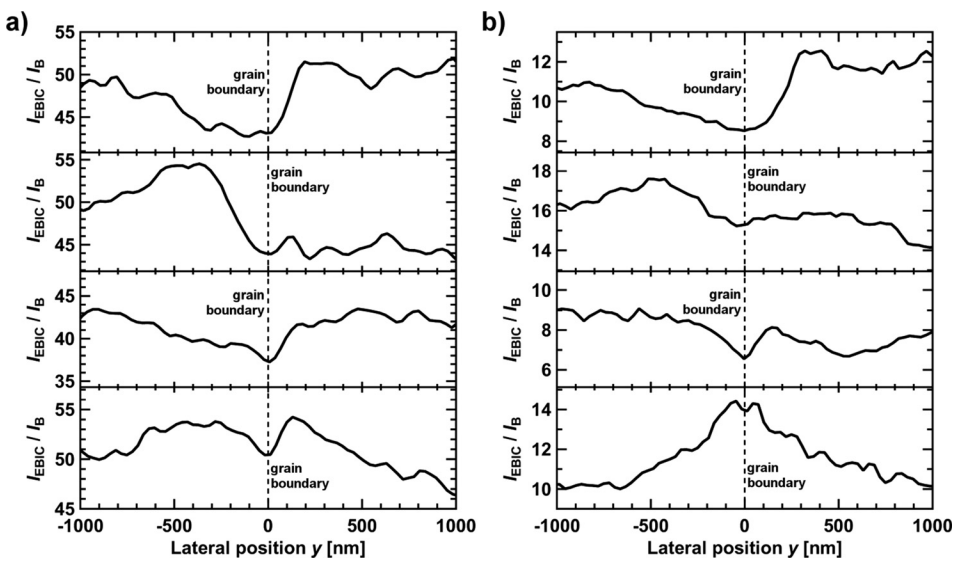

FIG. 7. Profiles extracted from EBIC images recorded with an electron-beam energy of 8 keV at (a) CIGSe and (b) CISe GBs. All EBIC intensities were normalized by the beam current I_B.

in Sec. III, see Subsec. IV G further below, we are currently unable to provide an physical explanation for the increased EBIC at GBs.

E. EBIC, CL, and EBSD data from identical positions

SEM, EBIC, EBSD, and CL data acquired on an identical position on the back surface of a CISe thin film are shown in Fig. 8. The current values given by the EBIC images depend on the distance of the impinging electron beam to the contact wire and on whether the contact wire touches the back contact directly on the CISe (also CIGSe) surface or whether graphite is deposited on the absorber back contact. The EBIC signals acquired at 5 keV, 125 pA, and room temperature are higher with a graphite layer on the CISe (CIGSe) surface, likely because of the better conductivity and reduced surface recombination than for a CISe (CIGSe) thin film only. The monochromatic CL image (Fig. 8(c)) acquired at about 8 K, 8 keV, 1 nA, and at a wavelength of 1260 nm (band-gap energy of CISe) shows the spatial distribution of radiative recombination from the CISe absorber. We note that up to date, we have not been able to acquire CL images from CI(G)Se thin films at room temperature with decent signal-to-noise ratios, which would be necessary for correlation of EBIC and CL images obtained at temperatures similar to working solar cells under sunlight.

The EBSD maps represent the diffraction pattern quality (Fig. 8(d)) and the orientation distribution (Fig. 8(e)) of the grains at the CISe back surface. At the position of the grain boundaries, the pattern quality is very low (dark pixels) since EBSD patterns from neighboring grains superimpose. As a result, the added EBSD pattern cannot be indexed by the evaluation software. GBs can be classified by means of EBSD measurements, which provide the misorientations between all neighboring grains. The misorientation again is related to the symmetry of the GB. A highly symmetric type of GBs are those with a Σ value of 3 (the Σ value is explained in detail in Ref. 22). These Σ3 GBs are highlighted in the pattern-quality map by white lines. Identifying unambiguously the Σ values of larger than 3 is not possible for GBs in polycrystalline CIGSe (or CISe) thin films. Thus, in the following, GBs are divided into Σ3 (twin) and non-Σ3 (random) GBs.

The EBIC and CL signals are not homogenous within the CI(G)Se thin films (disregarding effects at GBs). They are different for neighboring grains and also vary inside individual grains. The different orientations of the grains may influence the rates of backscattered electrons via channeling effects, i.e., the EBIC signal is reduced in case more electrons are backscattered. However, the EBSD data indicates that even for grains which exhibit similar orientations, the EBIC and the CL signals are different. We attribute the considerable variations of the EBIC and CL signals, therefore, rather to slight differences in net doping of the CI(G)Se grain interiors.

From EBIC as well as from CL images obtained on the CISe thin film, profiles (Fig. 8(f)) were extracted across a random and a Σ3 GB. While EBIC signals were found to be reduced in some grains but enhanced in others (see Fig. 7),

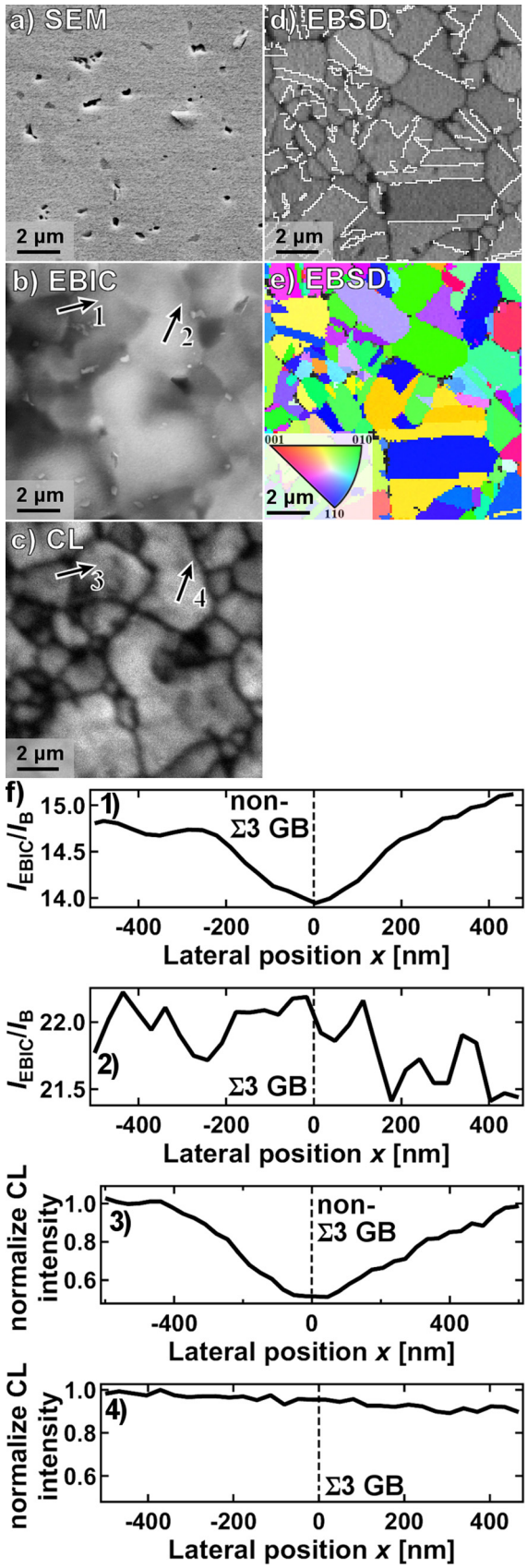

FIG. 8. SE image (a), EBIC image at 5 keV, 125 pA, and room temperature (b), CL image at 8 keV, 1 nA, 8 K and at 1260 nm (c), EBSD pattern quality map (d), and EBSD orientation distribution map (e), all acquired at the identical position of back surface of a $CuInSe_2$/CdS/ZnO stack as well as profiles across a non-Σ3 and a Σ3 GB (g). The white lines in the pattern-quality map (d) indicate the Σ3 GBs.

CL intensities were always found to be lower at random GBs (down to about 50 rel.%). Σ3 GBs do not exhibit any significant influence on both the EBIC and CL signals. The EBIC and CL signals across Σ3 and non-Σ3 GBs in CISe were found to be similar for other CIGSe thin films with different [Ga]/([Ga] + [In]) and [Cu]/([Ga]+[In]) ratios.[23]

Further CL images and a corresponding CL spectrum (Fig. 9) were recorded at about 8 K, 8 kV, and 1 nA. The images were acquired for various wavelengths between 1230 and 1510 nm (corresponding to 1.01 and 0.82 eV) on the same identical specimen position as that in Fig. 8. Outside of this wavelength range, the CL images do not exhibit signals above the noise level, as it is also apparent from the CL spectrum. Throughout the wavelength range between 1230 and 1510 nm, CL intensities were found to be decreased at non-Σ3 GBs with respect to the signals in grain interiors. The band-gap energy of CISe is about 1.04 eV at room temperature,[24] increasing to about 1.05 eV at 8 K.[25] The local maxima in the CL spectrum are positioned at 0.90 and 0.97 eV (1377 and 1283 nm), which can be related[26] to donor-acceptor pair transitions. The CL results in the present work do not indicate any preferential luminescence at the GBs with respect to the grain interiors.

F. Discussion of EBIC and CL results

Regarding the EBIC and CL signals at non-Σ3 GBs in CI(G)Se thin films, different signal distributions were found at different GBs. This situation indicates various electrical properties at these GBs, i.e., various densities of states. Different signal distributions at different non-Σ3 GBs in CI(G)Se thin films have also been obtained by correlated EBSD and Kelvin-probe force microscopy measurements given insight on work functions and energy-band bending,[27,28] by electron energy-loss spectrometry[29] and inline electron holography measurements performed in the transmission electron microscope,[30] providing compositional changes, as well as by scanning tunneling microscopy[31] probing the transport across GBs.

Within the scope of the present work, such a complex scenario with different EBIC and CL signal distributions at different non-Σ3 GBs in CIGSe thin films has been identified for various [Ga]/([In]+[Ga]) (ranging from 0 to 1) and [Cu]/([In]+[Ga]) ratios (from 0.6 to 0.9). Thus, this situation seems independent of the composition, at least in the ranges given above.

For non-Σ3 GBs at which local minima in the EBIC and CL images were detected, these reduced signals may be explained by a higher fraction of non-radiative recombination (e.g., by higher densities of defects, leading to midgap states and corresponding transitions) and also by reduced generation (e.g., due to larger band-gap energy) at these GBs. In contrast, for the GBs at which EBIC signals were found to be enhanced, a higher fraction of non-radiative recombination at GBs would be not probable. One possible scenario consistent with EBIC and CL obtained at all non-Σ3 GBs would be a larger band-gap energy than in the grain interiors.

From the series of CL images acquired at various wavelengths, it seems at first glance that no spectral shift is present between grain interiors and GBs. Indeed, such a behavior has also been detected by other CL measurements on CIGSe thin films.[32,33] However, the CL images do not

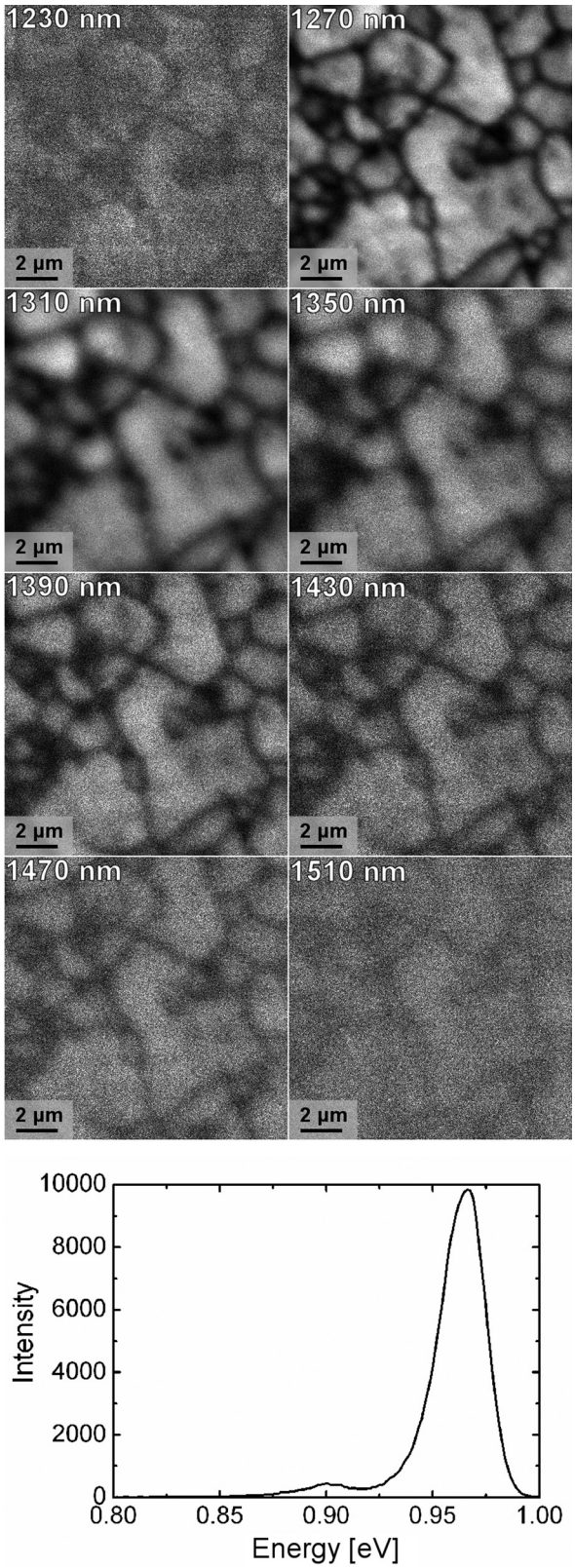

FIG. 9. Monochromatic CL images acquired at various wavelengths between 1230 nm and 1510 nm (8 kV, 1 nA, 8 K) on the same identical position as shown in Fig. 8, at the back surface of a CISe/CdS/ZnO stack, and a corresponding spectrum.

contain any information on from which position CL was emitted in the specimen (only the position of the impinging electron beam is known). It may be that the band-gap energy at GBs is larger (or smaller) than in the grain interiors, and generated charge carriers would diffuse to the position of the smallest band-gap energy before recombining and luminescence emission. Thus, no conclusions on the band-gap energy at a non-Σ3 GB in a CIGSe thin film can be drawn from the EBIC and CL measurements.

To date, it is still not clear how the energy-band diagram at an arbitrary, non-Σ3 GB looks like, including also defect states in the band gap. Thus, it cannot be concluded on the impact of non-radiative recombination and generation at non-Σ3 GBs in CIGSe thin films. This would need calculations by density-functional theory and multidimensional device simulations, both varying the compositional and electrical properties of the GBs.

G. Quantification of EBIC signals at GBs

In order to determine the diffusion length L and the recombination velocity S_{BC} at the back contact of a solar cell, EBIC measurements at different electron-beam energies E_B and thus different information depths are necessary. The procedure is described in Ref. 10. In order to take losses via shunting paths and series resistances into account, a collection efficiency Σ can be defined as $\Sigma = c\ (E_{eh}\ I_{EBIC})/(E_B\ I_B)$. The losses in the cell are described by a factor c, while E_{eh} is the energy to generate an electron-hole pair,[34,35] and I_{EBIC} is the measured or calculated current. Thus, together four variables influence the value of the current in dependence of the electron-beam energy E_B.

Measured and calculated collection efficiencies are shown in Fig. 10 for a $CuInSe_2$/CdS/ZnO stack, where EBIC images were acquired on the back surface of the CISe layer. The width w_{SCR} of the SCR was estimated by a complementary capacitance measurement and using $w_{SCR} = (\varepsilon_0 \varepsilon_r A)/C$ (with ε_0 and $\varepsilon_r = 11.1$ (Ref. 36) being the dielectrical permeabilities of vacuum and CISe, A the solar-cell area, and C the capacitance value) to about (570 ± 90) nm. The diffusion length L determined from EBIC measurements is about 300 nm, the recombination velocity S_{BC} at the back contact about 8×10^4 cm/s, and the factor for cell losses is $c = 0.26 \pm 0.04$. To show the influence of the parameters, in each graph in Figs. 10(a)–10(d), one of these is varied. The solid line in all graphs shows the best fit, which is not congruent with the measured data for all E_B. The higher slope of the measured data for $E_B > 16$ keV, and the following bend of the curve cannot be approximated well by the simulations. The higher slope is the result of the irradiation effect, as described in Sec. IV C.

Nevertheless, the extracted diffusion length L can be used as an approximation to estimate the effective diffusion length L_{eff} (Eq. (3)) and finally to simulate the current distribution across a GB. The collection efficiency is calculated for both the simulation and the measured data. In Fig. 11, measured and simulated collection efficiencies are shown for one CISe GB at $E_B = 4$ and 6 keV. The estimated recombination velocity S_{GB} is in the range of about 10^3 cm/s, but the width of the simulated collection efficiencies is wider than the measured. Thus, with this simple model applied, it is not possible to provide a decent fit of simulation and experiment.

We found that one approach for a better fit of the simulated and measured current distributions across CISe GBs is to assume a lower generation at the GB, as already suggested in the discussions given in Sec. IV F. A corresponding width has to be assumed for the GB region as further parameter. For recombination velocities of >0 cm/s, the decrease in EBIC at the GB would be higher assuming a band-gap energy of $E_g = 1.3$ eV at the GB than assuming $E_g = 1.04$ eV (band-gap energy of CISe (Ref. 20)). Thus, the simulation corresponds better to the measured data in Fig. 11. The estimated recombination velocity at this GB, assuming its width to be 20 nm, is in the range of $S_{GB} = 2.5 \times 10^3$ cm/s, which agrees well

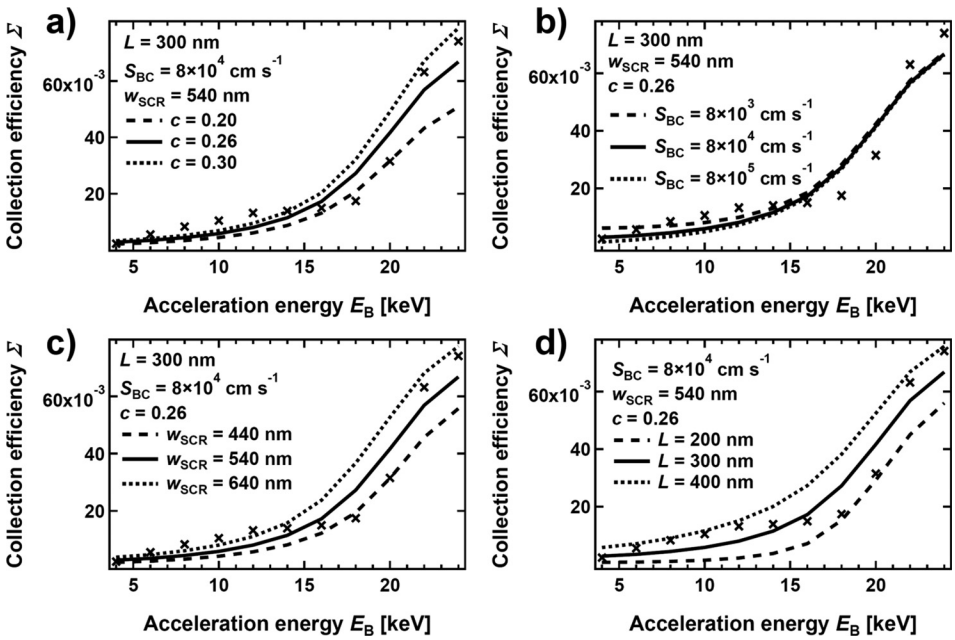

FIG. 10. Measured (marked with cross) and calculated collection efficiencies for a $CuInSe_2$ solar cell investigated from the back contact with varied (a) diffusion length L, (b) recombination velocity at the back contact S_{BC}, (c) width of the SCR, and (d) cell losses (c). The solid line in all diagrams represents the best fit to the measured data.

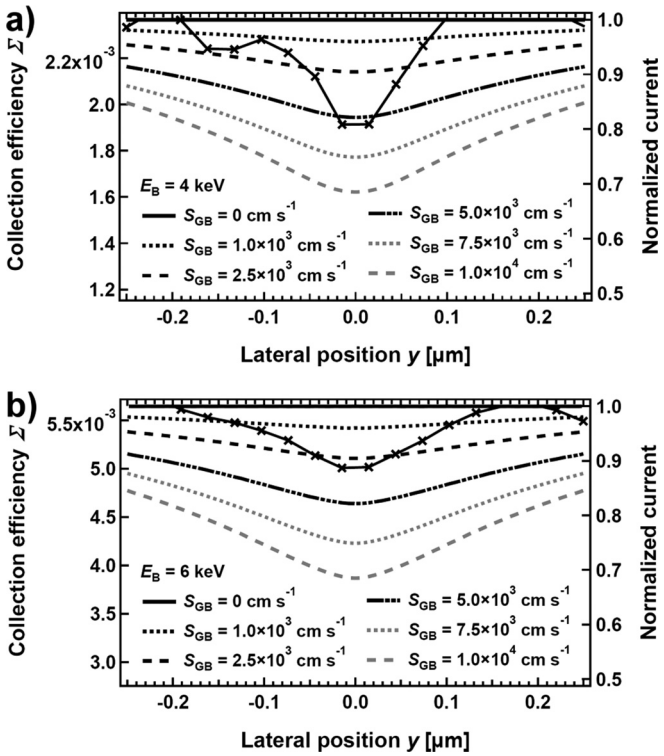

FIG. 11. Measured (marked by crosses) and simulated collection efficiency Σ for various S_{GB} at a CISe GB for $E_B = 4$ keV (a) and 6 keV (b).

with results from EBIC studies on cross-sectional solar-cell specimens.[6] The comparison between the widths of measured and the simulated EBIC profiles around the GB in Fig. 12 suggests that the spatial resolution in the EBIC experiment is not better than about 50 nm.

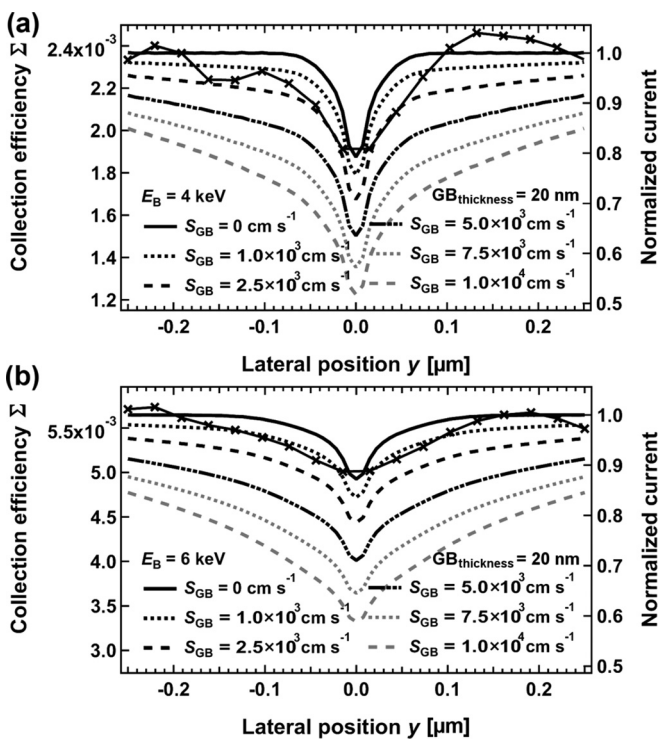

FIG. 12. Measured (marked by crosses) and simulated collection efficiency Σ for various S_{GB} at one CISe GB for $E_B = 4$ keV (a) and 6 keV (b).

However, with the additional parameters band-gap energy at the GB (and thus change in the generation rate of electron-hole pairs) as well as the width of the GB, a total number of six simulation parameters have to be varied to fit the simulated curves to the ones given in Fig. 11. Even taking these additional parameters into account, it was not possible to reproduce the experimental data satisfactorily in the present work. Also, the model presented above is not able to simulate decently all EBIC profiles across non-Σ3 GBs obtained in the present work (see, e.g., those in Fig. 7). Especially for the EBIC profiles with local maxima at the GBs, no physically reasonable model can be provided by the authors. Thus, the one-dimensional model applied in the present work seems not to be appropriate entirely for simulating the EBIC profiles across non-Σ3 GBs in CIGSe thin films. This issue needs further investigations by means of multidimensional device simulations.

V. CONCLUSIONS

It was shown that with a simple specimen preparation approach, the backside of CIGSe/CdS/ZnO stacks can be exposed for analysis by SEM techniques. Correlated EBIC, CL, and EBSD measurements on identical positions in the SEM are helpful tools to investigate the influence of the grain orientations and GBs on charge-carrier collection and radiative recombination.

For the sample series with various [Ga]/([In]+[Ga]) and [Cu]/([In]+[Ga]) ratios, the EBIC as well as the CL signals are inhomogeneous. They vary from grain to grain and also within individual grains. There was no correlation between the local orientation and the measured EBIC and CL signals. It was shown that at non-Σ3 GBs, local minima in CL signals and local minima as well as maxima in EBIC signals are present, and that Σ3 GBs show no significant influence on the short-circuit current and the radiative recombination. Overall, various behaviors of the EBIC and CL signals at different non-Σ3 GBs were detected. In case EBIC signals at non-Σ3 GBs are reduced, the corresponding values are only about 5 rel.% with respect to the values in the grain interiors. No conclusions are possible on the energy-band diagram at non-Σ3 GBs in CIGSe thin films. A model based on charge carriers diffusing to the GB, where they recombine, is only able to simulate EBIC profiles with local minima at non-Σ3 GBs if the generation is assumed to be reduced by 30%. Further two-dimensional device simulations are necessary to gain a better understanding of the EBIC signal distributions at GBs in CIGSe solar cells.

ACKNOWLEDGMENTS

The authors are grateful to Bianka Bunn, Jan Schniebs, Tim Münchenberg, Lars Steinkopf, Carola Ferber, Michael Kirsch for assistance in the production of the solar cells and to Jürgen Bundesmann for his SEM support. This work was supported in part by the BMU projects comCIGS and comCIGSII. R.C. acknowledges financial support from Spanish MINECO within the program Ramon y Cajal (RYC-2011-08521).

[1]A. Chirilă, P. Reinhard, F. Pianezzi, P. Bloesch, A. R. Uhl, C. Fella, L. Kranz, D. Keller, C. Gretener, H. Hagendorfer, D. Jaeger, R. Erni, S. Nishiwaki, S. Buecheler, and A. N. Tiwari, Nature Materials **12**, 1107 (2013).
[2]P. Jackson, D. Hariskos, E. Lotter, S. Paetel, R. Wuerz, R. Menner, W. Wischmann, and M. Powalla, Prog. Photovoltaics **19**, 894 (2011).
[3]K. Orgassa, U. Rau, H.-W. Schock, and J. H. Werner, in Proceedings of the 3rd World Conference on Photovoltaic Energy Conversion, Osaka, Japan, May 11–18, 2003 (Arisumi Printing Inc, Japan, 2003), p. 372.
[4]M. Nichterwitz, D. Abou-Ras, K. Sakurai, J. Bundesmann, T. Unold, R. Scheer, and H. W. Schock, Thin Solid Films **517**, 2554 (2009).
[5]M. Kawamura, T. Yamada, N. Suyama, A. Yamada, and M. Konagai, Jpn. J. Appl. Phys., Part 1 **49**, 062301 (2010).
[6]M. Nichterwitz, D. Abou-Ras, J. Kavalakkatt, R. Caballero, C. A. Kaufmann, T. Unold, R. Scheer, and H. W. Schock, "Electron-beam-induced current studies of grain boundaries in Cu(In,Ga)Se_2 thin-film solar cells" (unpublished).
[7]M. Nichterwitz and T. Unold, J. Appl. Phys. **114**, 134504 (2013).
[8]C. Donolato, Appl. Phys. Lett. **43**, 120 (1983).
[9]M. Nichterwitz, R. Caballero, C. A. Kaufmann, H.-W. Schock, and T. Unold, J. Appl. Phys. **113**, 044515 (2013).
[10]R. Scheer, Solid State Phenom. **67–68**, 57 (1999).
[11]D. Abou-Ras, S. Schorr, and H.-W. Schock, J. Appl. Crystallogr. **40**, 841 (2007).
[12]D. Abou-Ras, C. Koch, V. Küstner, C. Van Aken, U. Jahn, M. Contreras, R. Caballero, C. Kaufmann, R. Scheer, T. Unold, and H.-W. Schock, Thin Solid Films **517**, 2545 (2009).
[13]C. Kaufmann, A. Neisser, R. Klenk, and R. Scheer, Thin Solid Films **480**, 515 (2005).
[14]C. Donolato, J. Appl. Phys. **66**, 4524 (1989).
[15]D. J. Schroeder, J. L. Hernandez, G. D. Berry, and A. A. Rockett, J. Appl. Phys. **83**, 1519 (1998).
[16]T. E. Everhart and P. H. Hoff, J. Appl. Phys. **42**, 5837 (1971).
[17]J. Rechid, A. Kampmann, and R. Reineke-Koch, Thin Solid Films **361–362**, 198 (2000).
[18]H. J. Leamy, J. Appl. Phys. **53**, R51 (1982).
[19]M. Igalson and H.-W. Schock, J. Appl. Phys. **80**, 5765 (1996).
[20]J. T. Heath, J. D. Cohen, and W. N. Shafarman, J. Appl. Phys. **95**, 1000 (2004).
[21]S. Lany and A. Zunger, J. Appl. Phys. **100**, 113725 (2006).
[22]H. Grimmer, W. Bollmann, and D. H. Warrington, Acta Crystallogr., Sect. A: Cryst. Phys., Diffr., Theor. Gen. Crystallogr. **30**, 197 (1974).
[23]J. Kavalakkatt, Elektrische Eigenschaften von Chalcopyrithalbleitern, Master's thesis (in German), Technische Universität Berlin, Germany (2010).
[24]M. I. Alonso, K. Wakita, J. Pascual, M. Garriga, and N. Yamamoto, Phys. Rev. B **63**, 075203 (2001).
[25]A. V. Mudryia, I. A. Victorova, V. F. Gremenoka, A. I. Patuka, I. A. Shakina, and M. V. Yakushev, Thin Solid Films **431–432**, 197 (2003).
[26]S. Zott, K. Leo, M. Ruckh, and H. W. Schock, Appl. Phys. Lett. **68**, 1144 (1996).
[27]R. Baier, D. Abou-Ras, T. Rissom, M. C. Lux-Steiner, and S. Sadewasser, Appl. Phys. Lett. **99**, 172102 (2011).
[28]R. Baier, C. Leendertz, D. Abou-Ras, M. C. Lux-Steiner, and S. Sadewasser, "Properties of electronic potential barriers at grain boundaries in Cu(In,Ga)Se_2 thin films" (unpublished).
[29]D. Abou-Ras, B. Schaffer, M. Schaffer, S. S. Schmidt, R. Caballero, and T. Unold, Phys. Rev. Lett. **108**, 075502 (2012).
[30]D. Abou-Ras, S. S. Schmidt, R. Caballero, T. Unold, H.-W. Schock, C. T. Koch, B. Schaffer, M. Schaffer, P. Choi, and O. Cojocaru-Mirédin, Adv. Eng. Mater. **2**, 992 (2012).
[31]M. J. Romero, C.-S. Jiang, R. Noufi, and M. Al-Jassim, Appl. Phys. Lett. **87**, 172106 (2005).
[32]M. A. Contreras, I. Repins, W. K. Metzger, M. Romero, and D. Abou-Ras, Phys. Status Solidi. A **206**, 1042 (2009).
[33]M. Müller, D. Abou-Ras, T. Rissom, F. Bertram, and J. Christen, "Symmetry dependent optoelectronic properties of grain boundaries in polycrystalline Cu(In,Ga)Se_2 thin films," J. Appl. Phys. (unpublished).
[34]D. Holt and D. Joy, *SEM Microcharacterization of Semiconductors* (Academic Press, 1989).
[35]W. Ehrenberg and D. J. Gibbson, *Electron Bombardment Induced Conductivity and Its Applications* (Academic Press, 1981).
[36]C. Rincón, S. M. Wasim, and J. L. Ochoa, Phys. Status Solidi A **148**, 251 (1995).